Desalination and Water Treatment
www.deswater.com
doi: 10.5004/dwt.2021.27118

222 (2021) 209–218
May

Applications of dye adsorption in fixed bed column and modeling studies

Muhammed Onay, Çiğdem Sarıcı Özdemir*

Inonu University, Faculty of Engineering, Department of Chemical Engineering, Malatya, Turkey, Tel. +90 422 3774757; Fax: +90 422 3410046; email: cigdem.ozdemir@inonu.edu.tr (Ç.S. Özdemir)

Received 9 November 2020; Accepted 4 February 2021

ABSTRACT

In this study, adsorption studies of an aqueous solution of malachite green dye were made in a fixed bed using a thermal power plant. The effects of concentration, flow rate, adsorbent amount, and pH on adsorption applications were investigated. Thomas, Adams–Bohart and Yoon–Nelson models were used to evaluate the results obtained. In addition, the correlation between the model and the experimental data was compared using seven non-linear functions, while the adsorption dynamics of the fixed bed column were modeled. Scanning electron microscopy, X-ray diffraction, Fourier-transform infrared spectroscopy were used for the characterization of adsorbents. The results were compared with the results of previous studies and suggestions for adsorption applications were made accordingly. Yoon–Nelson models showed a good agreement with the experimental data. After the calculations, the maximum adsorption capacity of the fly ash dye was determined as 41.453 mg g^{-1}.

Keywords: Adsorption; Fixed bed column; Malachite green; Waste

1. Introduction

Dyes have many uses such as textiles, paper, printing, plastics. For example, malachite green is most commonly used for the dyeing of cotton, silk, paper, leather and also in manufacturing of paints and printing inks. It is difficult to remove malachite green (MG) from aqueous solutions and it is also toxic to important microorganisms. MG is used in many parts of the world because of its low cost, easy accessibility and reactivity, and alternatively because there is no more suitable product [1].

Chemical oxidation [2], foam flotation [3] adsorption [4], coagulation [5] electrodialysis [6] methods are used for dye removal from textile wastes. Adsorption is widely used for separation or purification in industrial processes. Because the dissolved dye compounds are self-supporting on the surface of the adsorbents, the dyes can be effectively treatment by adsorption In these studies, the balance and kinetic data in dye adsorption were examined [7,8]. One of the important parameters in the adsorption process is the adsorbent which is used. Agricultural and industrial wastes are used as adsorbents in adsorption processes. Fly ash is a waste material that comes in large quantities from modern power plants. The limited use of this waste area creates environmental problems with its cause. The use of fly ash as an adsorbent for industrial wastewater removal removes this problem in the first place. The main components of the power plant fly ash are silica (SiO_2), alumina (Al_2O_3) and iron oxides (Fe_2O_3), as well as carbon, calcium, magnesium and sulfur in different proportions [9].

Adsorption processes are carried out in fixed-bed columns in a continuous system. Continuous system fixed-bed columns are an efficient process for adsorption or desorption applications in periodically operated plants. Because the concentration of the dye in the input stream may vary. The main purpose of the column studies is; can predict the adsorption bed capacity at the time of adsorption columns or at the given column height, until reaching a predetermined output dye concentration [10–13].

* Corresponding author.

In this study, it was aimed to remove the malachite green from an aqueous solution by using fly ash in a fixed bed with a continuous flow system. Fly ash, which is quite abundant as thermal power plant waste and has high adsorption capacity in terms of surface properties, was chosen as the adsorbent in this study. Since the adsorption studies performed in batch systems provide a disadvantage in terms of time compared to continuous systems, column studies which are a continuous system have been examined. Important design parameters such as initial dye concentration, flow rate, adsorbent amount, pH value were investigated using a lab-scale fixed-bed column. The breakthrough curves for the adsorption of malachite green were analyzed using Adams–Bohart, Thomas and Yoon–Nelson models. In addition, the correlation between the model and the experimental data was measured by a non-linear error function when the adsorption dynamics of the fixed bed column were modeled.

2. Materials and methods

2.1. Materials

Fly ash was transferred to an oven set at 100°C for 24 h to reduce the water content. The dried sorbent was crushed and milled. The particle sizes were less than 200 mesh. Fly ash, obtained from Afşin Elbistan Thermal Power Plant, Kahramanmaraş, Turkey.

Malachite green (MG) (99.9% pure) was used as an adsorbate in this work. Malachite green is a cationic dye. MG has the molecular formula $C_{23}H_{25}ClN_2$ and the molecular weight of 364.92 g mol^{-1}. The spectrophotometric determination of MG was carried out using a Shimadzu UV-Vis spectrophotometer at 601 nm (Japan). Measurements in 5 mL of cuvettes were used.

2.2. Kinetic description in column

Continuous fixed-bed column studies were performed in a fixed bed mini-column reactor with an inside diameter of 2 cm, a column height of 50 cm. All experiments were carried out at 25°C. After almost 95%–98% exhaustion the column operation was stopped. The experiments performed are listed below;

2.2.1. Effect of initial dye concentration

Experiments were performed at three different starting dye concentrations, 50, 75 and 100 mg L^{-1}. The effect of the initial concentration was investigated by keeping the flow rate at 4 mL min^{-1}, pH value 4 and 5 g fly ash as adsorbent.

2.2.2. Effect of different adsorbent dosage

Experiments were carried out with three different adsorbents, 5, 7.5 and 10 g. The effect of the amount of adsorbent was investigated by keeping the flow rate at 4 mL min^{-1}, the pH value 4 and the initial dye concentration 75 mg L^{-1} constant.

2.2.3. Effect of flow rate

The experiments were carried out at two flow rates of 2 and 4 mL min^{-1}. The effect of flow rate was investigated by keeping the values constant such that the amount of adsorbent was 5 g fly ash, pH value 4 and initial dye concentration 75 mg L^{-1}.

2.2.4. Effect of the pH of the dye

The experiments were carried out at three different pH values, 2, 4 and 6. The effect of pH value was investigated by keeping the values constant at a flow rate of 4 mL min^{-1}, an initial dye concentration of 75 mg L^{-1} and an adsorbent amount of 5 g.

2.3. Adams–Bohart model

One of the kinetic expressions used in fixed bed adsorption studies is the Adams–Bohart model. The Adams–Bohart adsorption model was applied to describe the initial part of the breakthrough curve. This model assumes that the adsorption rate is proportional to both the residual capacity of the adsorbent and the concentration of dyes. The mass transfer rates obey the following equations:

$$\frac{dq}{dt} = -k_{AB} \cdot q \cdot C_{AB} \tag{1}$$

$$\frac{dC_b}{dz} = \frac{-k_{AB}}{U_0} \cdot q \cdot C_b \tag{2}$$

where k_{AB} is the kinetic constant (L mg^{-1} min^{-1}) and U_0 is the superficial velocity (cm min^{-1}). Some assumptions are made for the solution of these differential equation systems.

- Concentration field is considered to be low, for example, effluent concentration $C < 0.15\ C_0$;
- for $t \to \infty$ $q \to N_0$ (where N_0 is the maximum adsorption capacity (mg g^{-1}));

When the differential equation system is solved, the following equation is obtained with parameters k_{AB} and N_0.

$$\ln\frac{C}{C_0} = k_{AB} \cdot C_0 \cdot t - k_{AB} \cdot N_0 \frac{z}{U_0} \tag{3}$$

where C_0 and C are the inlet and effluent malachite green concentrations (mg L^{-1}), respectively [14,15].

2.4. Thomas model

The Thomas solution is used methods in fixed-bed column performance theory. The model has the following form:

$$\frac{C}{C_0} = \frac{1}{1 + \exp\left(\frac{k_{TH}}{Q}\left(q_0 \cdot X - C_0 \cdot V_{eff}\right)\right)} \tag{4}$$

where k_{TH} is the Thomas rate constant (mL min^{-1} mg^{-1}) and q_0 is the maximum solid-phase concentration of the solute (mg g^{-1}). The linearized form of the Thomas model is as follows:

$$\ln\left(\frac{C_0}{C}-1\right)=\frac{k_{TH}\cdot q_e\cdot X}{Q}-\frac{k_{TH}\cdot C_0}{Q}\cdot V_{eff} \quad (5)$$

The Thomas or reaction model assumes Langmuir kinetics of adsorption–desorption and no axial dispersion is derived with the adsorption that the rate driving force obeys second-order reversible reaction kinetics [16].

2.5. Yoon–Nelson model

Yoon–Nelson has developed a relatively simple model addressing the adsorption and breakthrough of adsorbate vapors of gases with respect to activated charcoal. The model is described on the assumption that the rate of decrease in the probability of adsorption for each adsorbate molecule is proportional to the probability of adsorbate adsorption and the probability of adsorbate breakthrough on the adsorbent. The Yoon–Nelson equation regarding a single-component system is expressed as:

$$\ln\frac{C}{C_0-C}=k_{YN}\cdot t-\tau\cdot k_{YN} \quad (6)$$

where k_{YN} is the rate constant (min^{-1}), t is the time required for 50% adsorbate breakthrough (min), and t is the breakthrough (sampling) time (min) [17].

2.6. Error analysis

In order to evaluate the fitness of the kinetic models to the experimental dynamic data, an error function is required to enable optimization procedure combining the values of determined coefficient (R^2) from the regressive analysis. In this study, the values of e were determined.

$$\varepsilon=\frac{\sum_{i=1}^{N}\left[\frac{\left(C/C_0\right)_{exp}-\left(C/C_0\right)_{th}}{\left(C/C_0\right)_{exp}}\right]}{N}\times 100 \quad (7)$$

where N is the number of measurements.

Linear regression analysis is one of the most appropriate means of determining the amount of dispersion of adsorbates and identifying the relationships in the adsorption system. It also allows mathematical analysis of adsorption systems. Non-linear optimization provides a method of determining column model parameter values, but an error function analysis is required to evaluate the fit of the calculated values in the model to the experimental results. In this study, eight non-linear error functions (sum squares errors, hybrid fractional error function, Marquardt's percent standard deviation, average relative error, sum of absolute error, the coefficient of determination, non-linear chi-square test) (Table 1) were investigated for malachite green adsorption onto fly ash.

3. Result and discussion

3.1. Pore structure characterization of the fly ash

The scanning electron microscopy (SEM) analysis of the fly ash is shown in Fig. 1. When the figure is examined, it is observed that there are needle-like structures on the surface of the fly ash that will form binding matrices. Soft spherical ash particles are in the structure. The mesoporous structure is indicative of its usefulness in fly ash adsorption studies [18].

The Fourier-transform infrared spectroscopy (FTIR) analysis of fly ash is shown in Fig. 2 (1000 FTIR Spectrophotometer of Mattson brand was used). The broad peak at about 3,400 cm^{-1} is due to the carbon O–H stretching vibration. The peak at about 1,000 cm^{-1} can be explained by the C–O tensile vibration. Peaks at about 1,400 to 1,600 cm^{-1} are due to asymmetric and symmetrical stretching vibrations of the $–CH_2–$ groups [19,20].

The crystalline phases of calcite, illite and quartz in fly ash are observed in Fig. 3. In the X-ray diffraction (XRD) graph, the peak of the quartz peaked at around 28° [21].

3.2. Effect of the initial dye concentration

According to Fig. 4, the breaking time increased as the initial dye concentration decreased. As the inlet concentration decreases, a long fracture curve is obtained, indicating that the solution can be processed at a higher volume. As the input dye concentration increased, sharper fracture curves were obtained. This is related to the pore structure of the adsorbent. While the mesopores in the structure filled later at lower concentrations, this time decreased as the concentration increased [22].

3.3. Effect of the adsorbent dosages

Fig. 5 shows that as the amount of adsorbent (bed height) increases, MG has more time to contact fly ash, resulting in a higher dye removal yield of MG. As the amount of adsorbent increases, the slope of the fracture curve decreases, which causes the mass transfer zone to expand. With the increase in the amount of adsorbent, the dye solution has spent more time on the fixed bed [23].

3.4. Effect of the flow rate

When Fig. 6 is examined, the breaking is faster as the flow rate increases. The transit time to saturation was significantly increased with the decrease in flow rate. At low flow rates, MG has spent more time in contact with the adsorbent and therefore causes more adsorption of MG molecules in the vicinity. Despite the fact that the adsorption of MG is a rapid process, the diffusing effects are lower due to the inadequate coloring of the column at high flow rates.

3.5. Effect of the initial pH

According to Fig. 7, as the pH of the dye increases, the break time decreases. As the pH decreases, a long fracture curve is obtained, indicating that the solution can be processed in a higher volume. As pH is increased, more sharp fracture curves are obtained.

3.6. Modelling of the breakthrough curves

3.6.1. Adams–Bohart model

The Adams–Bohart model was applied to the experimental data according to the initial dye concentration,

Table 1
List of error functions

Error function	Abbreviation	Definition
Sum of squares errors	ERRSQ	$\sum_{i=1}^{p}\left(q_{\exp}-q_{\text{cal}}\right)_i^2$
Hybrid fractional error function	HYBRID	$\frac{100}{p-n}\sum_{i=1}^{p}\left[\frac{\left(q_{\exp}-q_{\text{cal}}\right)^2}{q_{\exp}}\right]_i$
Marquardt's percent standard deviation	MPSD	$100\left[\sqrt{\frac{1}{p-n}\sum_{i=1}^{p}\left(\frac{q_{\exp}-q_{\text{cal}}}{q_{\exp}}\right)_i^2}\right]$
Average relative error	ARE	$\frac{100}{p}\sum_{i=1}^{p}\left(\frac{\left\|q_{\exp}-q_{\text{cal}}\right\|}{q_{\exp}}\right)_i$
Sum of absolute error	EABS	$\sum_{i=1}^{p}\left\|q_{\exp}-q_{\text{cal}}\right\|_i$
Coefficient of determination	R^2	$\frac{\left(q_{\exp}-\overline{q_{\text{cal}}}\right)^2}{\sum\left(q_{\exp}-\overline{q_{\text{cal}}}\right)^2+\left(q_{\exp}-q_{\text{cal}}\right)^2}$
Non-linear chi-square test	χ^2	$\sum_{i=1}^{p}\frac{\left(q_{\exp}-q_{\text{cal}}\right)^2}{q_{\exp}}$
Standard deviation of relative errors	S_{RE}	$\sqrt{\frac{\sum_{i=1}^{p}\left[\left(q_{\exp}-q_{\text{cal}}\right)_i-\text{ARE}\right]_i^2}{p-1}}$

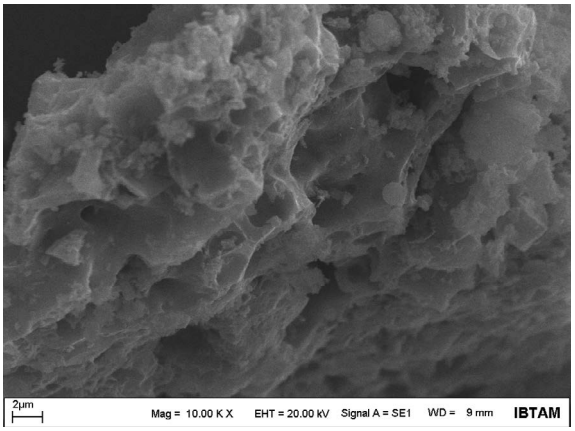

Fig. 1. Scanning electron microscopy analysis of adsorbent.

adsorbent amount, flow rate and different pH values. In order to determine the Adams–Bohart model parameters of N_0 and k_{AB}, non-linear regression analysis was used for each data set. When the MG concentration is increased to 50 and 100 mg L^{-1}, the k_{AB} and N_0 values are shown in Table 2. The experimental data are shown in Fig. 8a. Table 2. It is seen that the Adams–Bohart model has a higher correlation coefficient at low concentrations. As the concentration increases, the correlation coefficient decreases.

Investigation of the Adams–Bohart model based on the amount of adsorbent Fig. 8b. When the figure is examined, it is seen that experimental and theoretical values give closer curves to each other as the quantity increases. It can be seen that higher k_{AB} and N_0 values are obtained when 7.5 g of adsorbent is used.

Experimental data consistency of Adams–Bohart model due to pH change Fig. 8d. A better fit was observed as the pH value increased. Table 2 the k_{AB} value increases with increasing pH value.

In Fig. 8d, the results obtained at different flow velocities are compared with the theoretical model of Adams–Bohart and experimental values. When the shape is examined, the compatibility of the experimental data with the Adams–Bohart model is better at high flow rates. Adams–Bohart constants given in Table 2 show lower values with increasing flow rate.

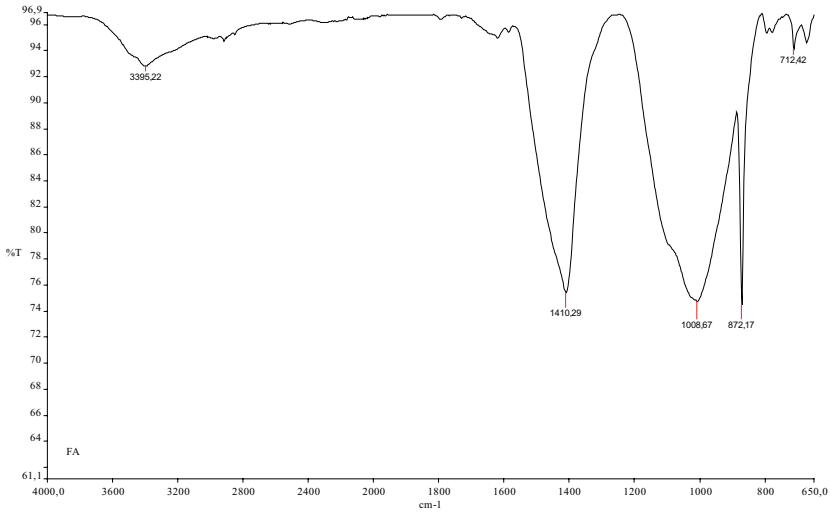

Fig. 2. Fourier-transform infrared spectroscopy analysis of adsorbent.

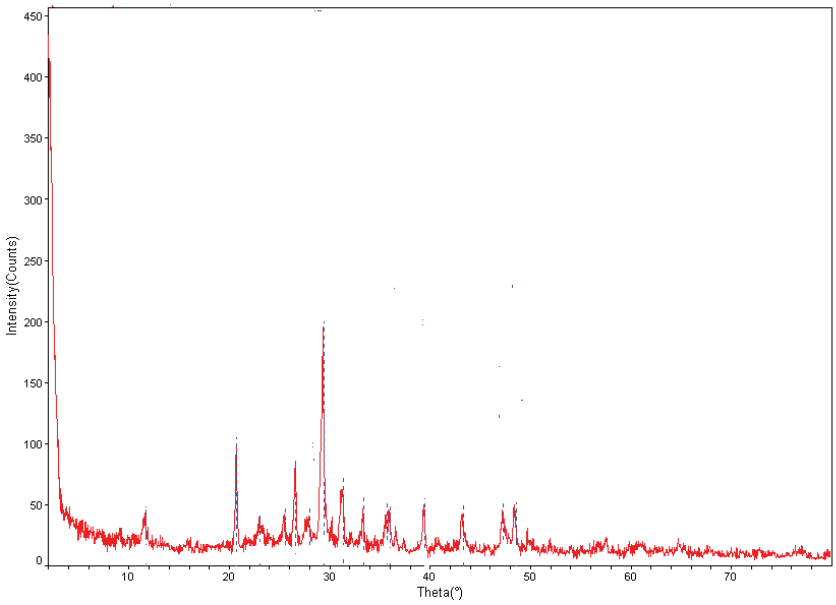

Fig. 3. X-ray diffraction analysis of adsorbent.

3.6.2. Thomas model

The Thomas model was applied to the effects of different parameters in the adsorption experiments. Comparison of the results obtained by changing the dye concentration with the Thomas model and experimental data is given in Fig. 9a. When the figure is examined, there is general agreement between concentration change and theoretical and experimental data. This compliance is better observed at 75 mg L^{-1} concentration. Thomas model constants and ε (%) values are given in Table 2. With increasing concentration, the adsorption capacity increases in q_0 (mg g^{-1}).

Comparison of Thomas model and experimental values are given in Fig. 9b depending on the amount of adsorbent. In general, the theoretical and empirical facts are consistent. When Table 2 where Thomas model constants are included increases the adsorption capacity q_0 (mg g^{-1}) with the increasing adsorbent amount.

Comparison of theoretical and experimental data at different pH values is given in Fig. 9c. When the graph is examined, when the dye is studied at the natural pH value of 4, the theoretical values and the experimental values are found to be more in harmony. Depending on the pH change of the functional groups in the structure, deviations occurred at low or high pH values. The Thomas model constants for the study with pH are given in Table 2. q_0 values are calculated as 19.765, 22.114, and 24.343 mg g^{-1}, respectively.

Comparisons of experiments at 2 and 4 mL min^{-1} flow rates are given in Fig. 9d. When the shape is examined, it is observed that the flow velocity does not make a difference

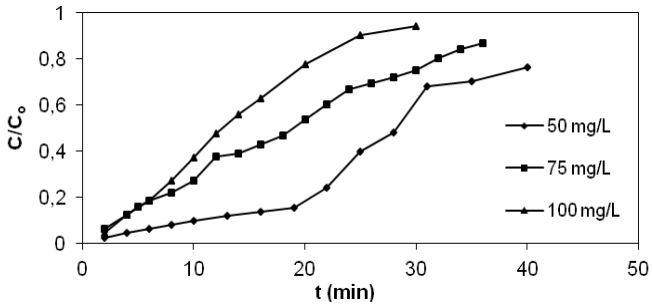

Fig. 4. Breakthrough curves of MG at various initial concentrations (m = 5 g; V = 4 mL min^{-1}; pH = 4).

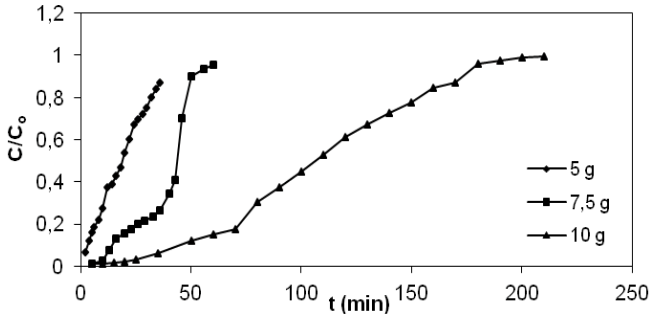

Fig. 5. Breakthrough curves of MG at various adsorbent dosages (C_0 = 75 mg L^{-1}; V = 4 mL min^{-1}; pH = 4).

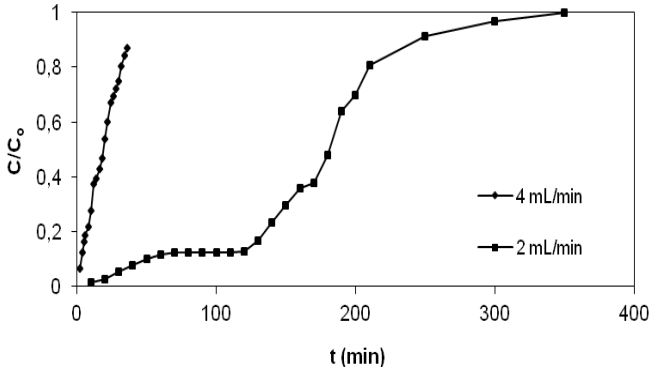

Fig. 6. Breakthrough curves of MG at various flow rates (C_0 = 75 mg L^{-1}; m = 5 g; pH = 4).

in terms of the compatibility between experimental values and theoretical values.

3.6.3. Yoon–Nelson model

The Yoon–Nelson model applied different adsorbent amounts, MG initial concentration, pH and flow rate to the experimental data. Non-linear regression analysis is used in each data set to determine the Yoon–Nelson model parameters and τ and k_{YN} values are calculated. The graph of the data obtained by applying the Yoon–Nelson model with the experimental data is shown in Fig. 10a are shown. When the figure is examined, the theoretical and experimental values have become more regular in varying concentrations. τ values are calculated as 361.99, 228.33 and 273.4 min, respectively.

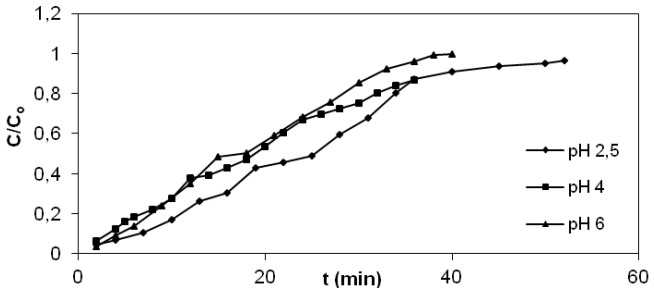

Fig. 7. Breakthrough curves of MG at various initial pH (C_0 = 75 mg L^{-1}; m = 5 g; V = 4 mL min^{-1}).

Comparison of experimental and Yoon–Nelson model data using 5, 7.5 and 10 g of fly ash is given in Fig. 10b. When 5 g fly ash is used, the theoretical and experimental values show a better fit. When the table was examined, the correlation coefficients of 5 g and 10 g were very high. However, when 5 g is used, the reaction rate constant value is set to 0.186 (min^{-1}). Since this value is higher than 10 g, studies with 5 g are more suitable.

Comparison with varying pH values is given in Fig. 10c for the Yoon–Nelson model and in Table 2 in the parameter values. When the figure is examined, it is seen that working at natural pH value gives better results.

The effect of flow rate is given in Fig. 10d. As in other theoretical models, the Yoon–Nelson model shows that both flow velocities are consistent with experimental values. At a flow rate of 4 mL min^{-1}, the higher correlation coefficient and the higher reaction rate constant were calculated, while the residence time was lower.

3.7. Error functions for modeling

In contrast to the linearization models, non-linear regression usually involves minimizing the error distribution based on convergence criteria, or the maximum distribution (between the experimental data and the model predicted).

In this study, seven non-linear error functions (stability coefficient (R^2), the sum of squares errors (ERRSQ), hybrid fractional error function (HYBRID), average relative error (ARE), the sum of absolute error (EABS), Marquardt's percent standard deviation (MPSD), non-linear χ^2 test (χ^2)) were applied to experimental data for Adams–Bohart, Thomas and Yoon–Nelson models. The results are given in Table 3.

Table 3 when considering the initial concentration of the dye, all error functions agree with the Yoon–Nelson model. The highest values according to the correlation coefficient (R^2) are found in the Yoon–Nelson model. The error values are calculated less for the Yoon–Nelson model, despite varying concentrations when ERRSQ, HYBRID, ARE, EABS, MPSD and χ^2 error functions are considered.

It is seen in Table 3 that the correlation coefficients are increased with application of the data obtained in the experiments using 5, 7.5 and 10 g of fly ash and Yoon–Nelson model and the minimum amount of other error function values are obtained in Yoon–Nelson model. This is due to the fact that the Yoon–Nelson model is less complicated

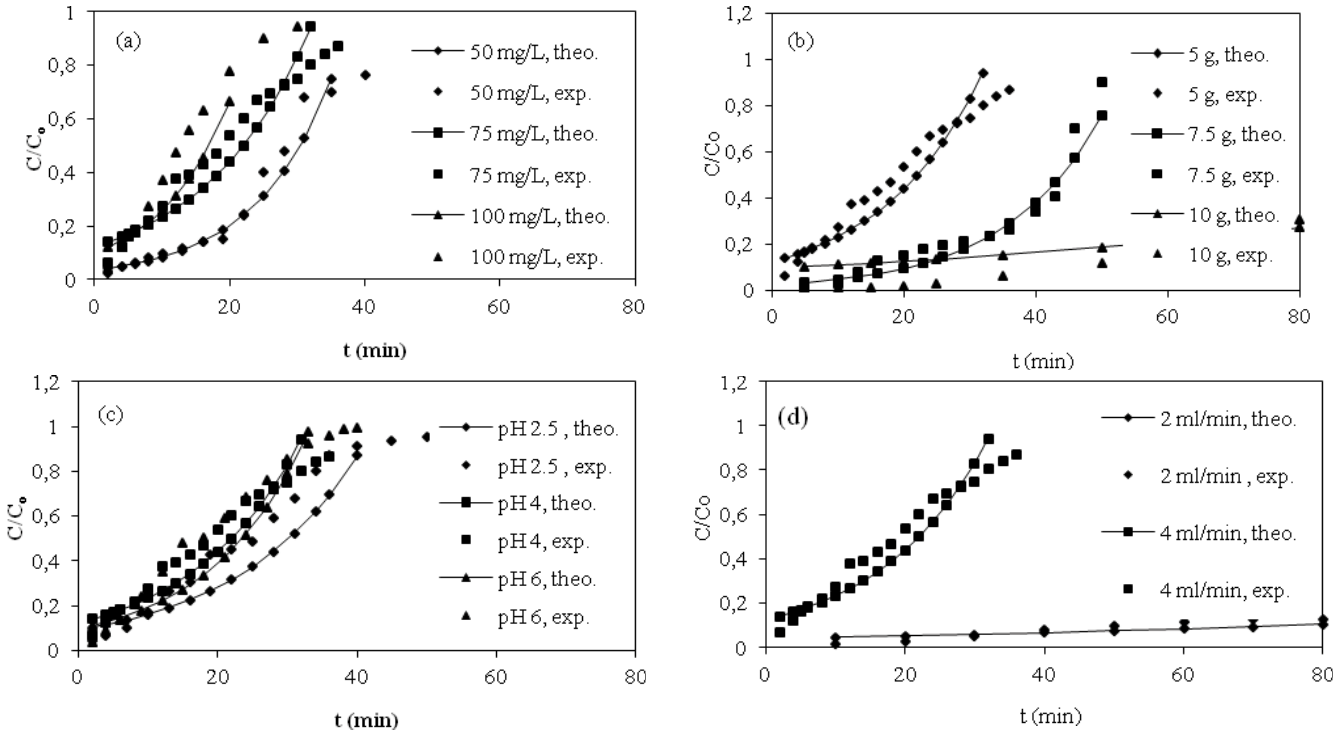

Fig. 8. Predicted breakthrough curves of MG by the main form of Adams–Bohart model at (a) various inlet concentration of MG (m = 5 g; V = 4 mL min^{-1}; pH = 4), (b) various adsorbent dosages (C_0 = 75 mg L^{-1}; V = 4 mL min^{-1}; pH = 4), (c) various flow rates (C_0 = 75 mg L^{-1}; m = 5 g; pH = 4), and (d) at various initial pH (C_0 = 75 mg L^{-1}; m = 5 g; V = 4 mL min^{-1}), and comparison with experimental data.

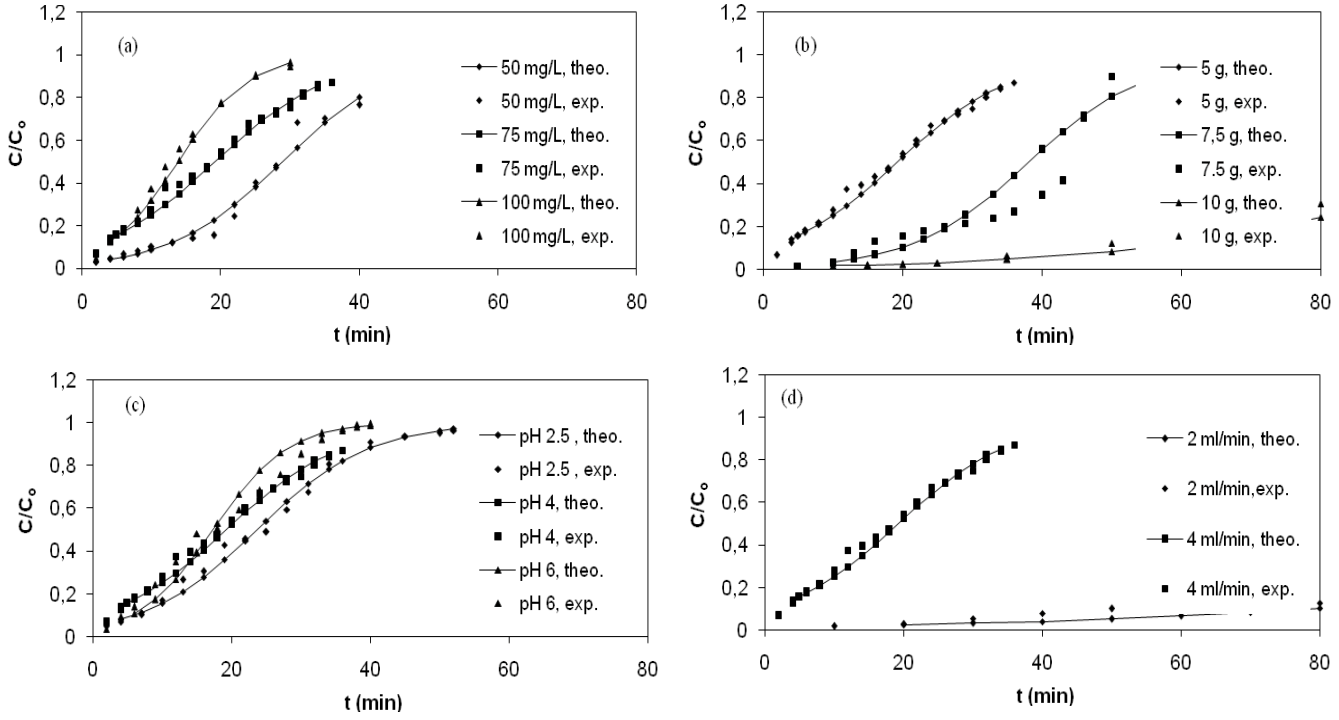

Fig. 9. Predicted breakthrough curves of MG by the main form of Thomas model at (a) various inlet concentration of MG (m = 5 g; V = 4 mL min^{-1}; pH = 4), (b) various adsorbent dosages (C_0 = 75 mg L^{-1}; V = 4 mL min^{-1}; pH = 4), (c) flow rates (C_0 = 75 mg L^{-1}; m = 5 g; pH = 4), and (d) at various initial pH (C_0 = 75 mg L^{-1}; m = 5 g; V = 4 mL min^{-1}), and comparison with experimental data.

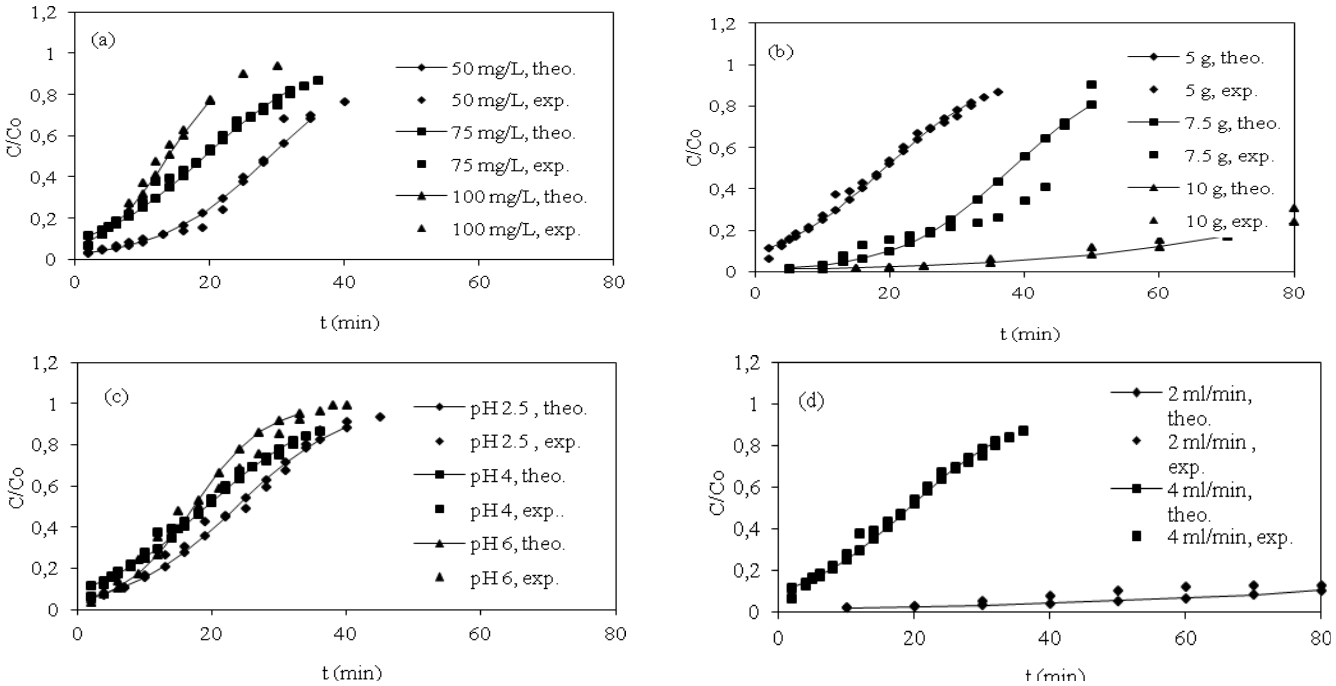

Fig. 10. Predicted breakthrough curves of MG by the main form of Yoon–Nelson model at (a) various inlet concentration of MG (m = 5 g; V = 4 mL min^{-1}; pH = 4), (b) various adsorbent dosages (C_0 = 75 mg L^{-1}; V = 4 mL min^{-1}; pH = 4), (c) various flow rates (C_0 = 75 mg L^{-1}; m = 5 g; pH = 4) and (d) at various initial pH (C_0 = 75 mg L^{-1}; m = 5 g; V = 4 mL min^{-1}), and comparison with experimental data.

Table 2
Constant of Adams–Bohart, Thomas, Yoon–Nelson models

		k_{AB} (mL min^{-1} mg^{-1})	N_0 (g L^{-1})	ε (%)	q_0 (mg g^{-1})	k_{TH} (mL mg^{-1} dak^{-1})	ε (%)	τ (min)	k_{YN} (min^{-1})	ε (%)
Concentration	50	0.0876	3,356.0	17.98	26.0995	0.1251	14.596	361.99	0.1251	13.572
(mg L^{-1})	75	0.0635	2,091.50	21.967	32.114	0.1186	9.215	228.33	0.1186	5.531
	100	0.0942	2,293.10	14.517	41.453	0.1971	14.517	273.4	0.1971	5.353
Adsorbent	5	0.0635	2,091.50	21.967	22.114	0.1186	9.215	228.33	0.1186	5.531
dosage (g)	7.5	0.0685	3,704.6	36.52	27.44	0.1206	30.25	359.81	0.1206	28.982
	10	0.0128	2,320.5	49.896	30.79	0.0423	10.214	453.16	0.0423	9.668
pH	2.5	0.0563	2,392.4	37.27	19.765	0.1246	9.165	295.04	0.1246	7.201
	4	0.0635	2,091.50	21.967	22.114	0.1186	9.215	228.33	0.1186	5.531
	6	0.0707	2,359.3	40.729	24.343	0.1886	14.81	327.25	0.1886	12.116
Flow rate	2	0.0119	3,196.0	38.179	38.651	0.0255	29.506	420.82	0.0255	30.641
(mL min^{-1})	4	0.0635	2,091.50	21.967	22.114	0.1186	9.215	228.33	0.1186	5.531

when we compare the other two models (Adams–Bohart and Thomas) and that the physical properties of the adsorbate are not effective in the adsorption even.

In the case of pH change, the Thomas model showed a higher correlation coefficient and lower error values than the Yoon–Nelson model at lower pH values.

When the correlation coefficient and the error function values of the flow rates of 2 and 4 mL min^{-1} are examined, the compliance is observed in the Yoon–Nelson model as in concentration and quantity [24–26].

4. Conclusion

In this study, dye works were done on the fixed bed by using fly ash as thermal power plant waste. The effect of concentration, flow rate, adsorbent amount, and pH on adsorption applications was investigated. Thomas, Adams–Bohart and Yoon–Nelson models were used to evaluate the results obtained. SEM, XRD, and FTIR methods were used for the characterization of adsorbents. When working at lower concentrations in the initial dye concentration, a more appropriate fracture curve is obtained, and as

Table 3
Error analysis

		Model	R^2	ERRSQ	HYBRID	ARE	EABS	MPSD	χ^2
		Adams–Bohart	0.956	0.198	2.905	2.490	0.128	5.745	0.295
	50 mg L^{-1}	Thomas	0.973	0.024	2.749	2.356	0.018	5.979	0.080
		Yoon–Nelson	0.974	0.019	2.453	2.014	0.014	3.125	0.145
		Adams–Bohart	0.869	0.274	4.302	3.849	0.134	48.904	0.477
Concentration	75 mg L^{-1}	Thomas	0.977	0.015	1.521	1.361	0.127	16.311	0.070
		Yoon–Nelson	0.984	0.013	1.113	1.056	0.089	11.236	0.069
		Adams–Bohart	0.769	0.732	13.970	11.430	0.216	46.030	1.009
	100 mg L^{-1}	Thomas	0.971	0.014	4.282	3.504	0.188	11.049	0.069
		Yoon–Nelson	0.981	0.013	3.865	2.726	0.144	9.112	0.056
		Adams–Bohart	0.869	0.274	4.302	3.849	0.134	48.904	0.477
	5 g	Thomas	0.977	0.015	1.521	1.361	0.127	16.311	0.070
		Yoon–Nelson	0.984	0.013	1.113	1.056	0.089	11.236	0.069
		Adams–Bohart	0.881	0.394	11.044	9.663	0.357	33.721	0.559
Dosage	7.5 g	Thomas	0.921	0.164	10.225	8.946	0.435	27.645	0.527
		Yoon–Nelson	0.918	0.139	0.812	6.761	0.182	19.456	0.470
		Adams–Bohart	0.867	0.437	13.011	11.566	0.227	27.860	0.713
	10 g	Thomas	0.983	0.033	0.908	0.807	0.121	9.968	0.078
		Yoon–Nelson	0.953	0.029	0.812	0.765	0.102	8.456	0.070
		Adams–Bohart	0.859	3.192	11.465	10.510	0.893	55.766	3.465
	2 mL min^{-1}	Thomas	0.946	0.121	9.141	8.379	0.682	42.769	0.564
Rate		Yoon–Nelson	0.964	0.112	6.453	6.243	0.240	31.445	0.380
		Adams–Bohart	0.869	0.274	4.302	3.849	0.134	48.904	0.477
	4 mL min^{-1}	Thomas	0.977	0.015	1.521	1.361	0.127	16.311	0.070
		Yoon–Nelson	0.984	0.013	1.113	1.056	0.089	11.236	0.069
		Adams–Bohart	0.835	1.117	9.423	8.314	0.388	25.949	1.407
	2.5	Thomas	0.986	0.018	1.477	1.304	0.082	3.701	0.049
		Yoon–Nelson	0.981	0.016	1.234	1.154	0.064	2.135	0.035
		Adams–Bohart	0.869	0.274	4.302	3.849	0.134	48.904	0.477
pH	4	Thomas	0.977	0.015	1.521	1.361	0.127	16.311	0.070
		Yoon–Nelson	0.984	0.013	1.113	1.056	0.089	11.236	0.069
		Adams–Bohart	0.799	0.759	13.587	11.776	0.313	41.290	1.092
	6	Thomas	0.955	0.051	0.351	0.304	0.104	7.271	0.119
		Yoon–Nelson	0.954	0.046	0.598	0.784	0.254	6.445	0.097

the concentration is increased, the fracture curve is sharpened. When we look at the effect of adsorbent amount on fixed bed operation; it has been observed that the time of adsorption and bedtime increase with increasing amount. It has been determined that the application of flow rate is an important parameter for determining the fracture curve and that low flow rates are not sufficient for this.

Acknowledgment

This work was supported by İnönü University Scientific Research Coordination Unit: Project Number: FYL-2017-618.

References

[1] A.K. Srivastav, S.K. Srivastava, A.K. Srivastava, Response of serum calcium and inorganic phosphate of freshwater catfish, *Heteropneustes fossilis*, to chlorpyrifos, Bull. Environ. Contam. Toxicol., 58 (1999) 915–920.
[2] I. Michael-Kordatou, P. Karaolia, D. Fatta-Kassinos, The role of operating parameters and oxidative damage mechanisms of advanced chemical oxidation processes in the combat against antibiotic-resistant bacteria and resistance genes present in urban wastewater, Water Res., 129 (2018) 208–230.
[3] Y. Lee, P. Wang, S. Lo, C.P. Huang, Recovery of perfluorooctane sulfonate (PFOS) and perfluorooctanoate (PFOA) from dilute water solution by foam flotation, Sep. Purif. Technol., 173 (2017) 280–285.
[4] Ç. Sarici-Özdemir, F. Kiliç, Kinetics behavior of methylene blue onto agricultural waste, Part. Sci. Technol., 36 (2018) 194–201.
[5] Z. Zhang, J. Wang, D. Liu, J. Li, X. Wang, B. Song, B. Yue, K. Zhao, Y. Song Hydrolysis of polyaluminum chloride prior to coagulation: effects on coagulation behavior and implications for improving coagulation performance, J. Environ. Sci., 57 (2017) 162–169.
[6] D. Babilas, P. Dydo, Selective zinc recovery from electroplating wastewaters by electrodialysis enhanced with complex formation, Sep. Purif. Technol., 192 (2018) 419–428.

[7] I. Anastopoulos, A. Mittal, M. Usman, J. Mittal, G. Yu, A. Núñez-Delgado, M. Kornaros, A review on halloysite-based adsorbents to remove pollutants in water and wastewater, J. Mol. Liq., 218 (2020) 855–868.
[8] C. Arora, S. Soni, S. Sahu, J. Mittal, P.K. Bajpai, Iron based metal organic framework for efficient removal of methylene blue dye from industrial waste, J. Mol. Liq., 284 (2019) 343–352.
[9] S.B. Wang, H.W. Wu, Environmental-benign utilisation of fly ash as low-cost adsorbents, J. Hazard. Mater., 136 (2006) 482–501.
[10] J.P. Chen, M.S. Lin, Equilibrium and kinetics of metal ion adsorption onto a commercial H-type granular activated carbon; experimental and modeling studies, Water Res., 35 (2001) 2385–2394.
[11] Z. Aksu, F. Gönen, Biosorption of phenol by immobilized activated sludge in a continuous packed bed: prediction of breakthrough curves, Process Biochem., 39 (2004) 599–613.
[12] J.R. Rao, T. Viraraghavan, Biosorption of phenol from an aqueous solution by *Aspergillus niger* biomass, Bioresour. Technol., 85 (2002) 165–171.
[13] M. Lehmann, A.I. Zouboulis, K.A. Matis, Modelling the sorption of metals from aqueous solutions on goethite fixed-beds, Environ. Pollut., 113 (2001) 121–128.
[14] A.C. Texier, Y. Andrès, C. Faur-Brasquet, P. Le-Cloirec, Fixed-bed study for lanthanide (La, Eu, Yb) ions removal from aqueous solutions by immobilized *Pseudomonas aeruginosa*: experimental data and modelization, Process Biochem., 47 (2002) 333–342.
[15] E. Guibal, R. Lorenzelli, T. Vincent, Application of silica gel to metal ion adsorption static and dynamic removal of uranyl ions, Environ. Technol., 16 (1995) 101–114.
[16] H.C. Thomas, Heterogeneous ion exchange in a flowing system, J. Am. Chem. Soc., 66 (1944) 1664–1666.
[17] W.T. Tsai, C.Y. Chang, C.Y. Ho, L.Y. Chen, Adsorption properties and breakthrough model of 1,1-dichloro-1-fluoroethane on activated carbons, J. Hazard. Mater., 69 (1999) 53–66.
[18] A.K. Saha, Effect of class F fly ash on the durability properties of concrete, Sustainable Environ. Res., 28 (2018) 25–31.
[19] A. Alswat Abdullah, B.A. Mansor, Z.H. Mohd, A.I. Nor, A.S. Tawfik, Copper oxide nanoparticles-loaded zeolite and its characteristics and antibacterial activities, J. Mater. Sci. Technol., 33 (2017) 889–896.
[20] F. Cataldo, M.V. Putz, O. Ursini, G. Angelini, Surface modification of activated carbon fabric with ozone. Part 2: Thermal analysis with TGA-FTIR and DTA, Fullerenes Nanotubes Carbon Nanostruct., 24 (2016) 400–405.
[21] S.R. Silva, J.J.O. Andrade, Investigation of mechanical properties and carbonation of concretes with construction and demolition waste and fly ash, Constr. Build. Mater., 153 (2017) 704–715.
[22] Ç. Sarıcı-Özdemir, Modeling of tartrazine adsorption onto activated carbon fiber in a continuous fixed-bed reactor, Desal. Water Treat., 46 (2012) 234–243.
[23] L. Sheng, Y. Zhang, F. Tang, S. Liu, Mesoporous/microporous silica materials: preparation from natural sands and highly efficient fixed-bed adsorption of methylene blue in wastewater, Microporous Mesoporous Mater., 257 (2018) 9–18.
[24] K.W. Jung, T.U. Jeong, J.W. Choia, K.H. Ahn, S.H. Lee, Adsorption of phosphate from aqueous solution using electrochemically modified biochar calcium-alginate beads: batch and fixed-bed column performance, Bioresour. Technol., 244 (2017) 23–32.
[25] V. Ponnusami, V. Gunasekar, S.N. Srivastava, Kinetics of methylene blue removal from aqueous solution using gulmohar (*Delonix regia*) plant leaf powder: multivariate regression analysis, J. Hazard. Mater., 169 (2009) 119–127.
[26] M.C. Ncibi, B. Mahjoub, M. Seffen, Kinetic and equilibrium studies of methylene blue biosorption by *Posidonia oceanica* (L.) fibres, J. Hazard. Mater., 139 (2007) 280–285.